

# Multiscale Electrothermal Simulation of Quantum Cascade Laser Operation

Irena Knezevic

University of Wisconsin – Madison, Madison, Wisconsin, USA

Contact email: iknezevic@wisc.edu

**Abstract** — Quantum cascade lasers (QCLs) are high-power coherent light sources in the midinfrared and terahertz parts of the electromagnetic spectrum. They are systems in which the electronic and lattice systems are far from equilibrium, strongly coupled to one another, and the problem bridges disparate spatial scales. We present our ongoing work on the multiphysics and multiscale simulation of far-from-equilibrium transport of charge and heat in QCLs.

Quantum cascade lasers (QCLs) are electrically driven, unipolar, coherent light sources in the midinfrared (mid-IR) and terahertz (THz) parts of the electromagnetic spectrum. In addition to being of great technological importance, QCLs are fascinating nonequilibrium systems that are typically thoroughly characterized via electrical, optical, and thermal measurements precisely because of their practical value. As a result, QCLs are excellent as model systems for far-from-equilibrium theoretical studies.

Under high-power, continuous-wave (CW) operation, the electron and phonon systems in QCLs are both very far from equilibrium and strongly coupled to one another, which makes them very challenging to accurately model. The problem of their coupled dynamics is both multiphysics (coupled electronic and thermal) and multiscale (bridging between a single stage and device level). During typical QCL operation, large amounts of energy are pumped into the electronic system, of which a small fraction is given back through the desired optical transitions, while the bulk of it is deposited into the optical-phonon system. Longitudinal optical (LO) phonons decay into longitudinal acoustic (LA) phonons; this three-phonon process is often referred to as anharmonic decay. LA phonons have high group velocity and are the dominant carriers of heat. Anharmonic decay is typically an order of magnitude slower than the rate at which the electron system deposits energy into the optical-phonon system. The fast relaxation of electrons into LO phonons, followed by the LO phonon slower decay into LA phonons, results in excess nonequilibrium optical phonons that can have appreciable feedback on electronic transport, population inversion, and the QCL figures of merit.

Figure 1 depicts typical energy flow in a quantum cascade laser. While electrical transport and optical-field emission occur in the active region of the device and can be electrically controlled, thermal transport involves the entire large device and is only controlled via thermal boundary conditions that can be far from the active region. As a result, different stages in the active region will have temperatures different from one another and drastically different from the heat sink (see Fig. 2). The electronic temperatures are higher still, differing among subbands, and affecting leakage paths and thus QCL performance. What is needed is a multiscale

electrothermal simulation to describe QCL performance in the far-from-equilibrium conditions of CW operation.

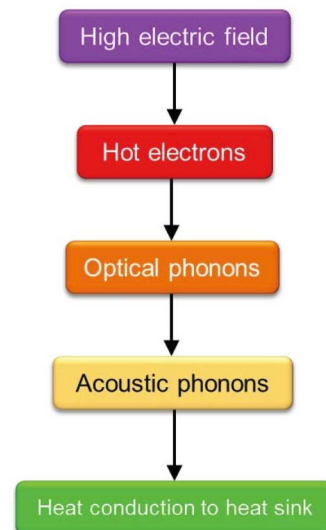


Figure 1. Flow of energy in a quantum cascade laser.

Figure 2 shows the schematic of a typical device structure (not to scale). Plasmonic waveguides (cladding layers) are typically employed in the mid-IR. As the “depth” of a QCL device (dimension normal to the page) is much greater than its width or height, we can carry out a 2D device-level electrothermal simulation. What we know (i.e., can measure or directly control in experiment) are: bias across the device, electrical current, and the temperature boundary conditions.

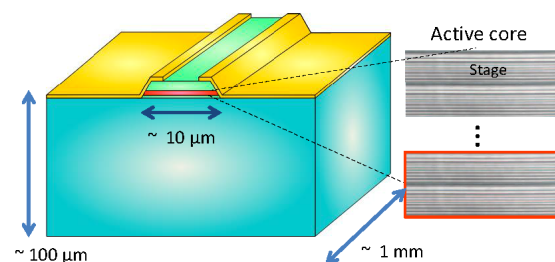


Figure 2. The multiscale nature of the QCL transport problem. While electron transport and optical-field emission occur in the active core of the device and can be electrically controlled, thermal transport involves the entire large device and is only controlled via thermal boundary conditions that can be far from the active core.

Typically, the bottom boundary of the device is connected to a heat sink while other boundaries have the convective boundary condition at the environment temperature (single-

device case) or the adiabatic (i.e., zero heat flux) boundary condition (array case).

Inside the active core, we cannot *a priori* tell much about the lattice temperature, other than qualitatively expecting an active region hotter than the rest of the device because of all the transfer of energy from the electron to the phonon system. In the same vein, there is no guarantee that the electric field will be uniform across different stages in the active core. In fact, electric-field variation between stages is a staple of superlattices]. What we *do* know is that the charge–current continuity equation must hold and that, if we approximate the current flow as 1D through the active core (vertical direction in Fig. 2), then the current must be constant in the steady state. This key insight informs the algorithm used for device-level electrothermal simulation (Fig. 3).

1) Based on single-stage simulation for an assumed electric field  $F$  and lattice temperature  $T_L$ , the latter coinciding with the acoustic-phonon-ensemble temperature.  $T_L$  gives baseline phonon occupations and electron–phonon scattering rates. For each field  $F$  and lattice temperature  $T_L$ , the output of single-stage simulation consists of electrical current density  $J$  and the heat-generation rate  $Q$ .  $Q$  is proportional to the rate at which acoustic phonons are generated by the decaying optical phonons and is easily recorded in single-stage simulation. By sweeping  $F$  and  $T_L$ , single-stage coupled simulation yields a “table” that links  $(F, T_L)$  pairs to appropriate  $(J, Q)$  pairs.

2) Current continuity. In the steady state, the current density  $J$  must be the same in every stage, so we use  $J$  as an input variable for the device-level simulation. Therefore we “flip” the table from  $(T_L, F) \rightarrow (J, Q)$  to  $(J, T_L) \rightarrow (Q, F)$ , which can really be thought of as a series of  $F$  vs.  $J$  and  $Q$  vs.  $J$  curves at different lattice temperatures. The flipped table  $(J, T_L) \rightarrow (Q, F)$  is key information needed from single-stage simulation for device-level simulation.

3) Heat flow through the whole device. In essence, the global simulation is the solution to the heat-diffusion equation, with each stage in the active core acting as a current-dependent heat source. The global heat diffusion equation is solved using finite elements. We do not know what temperature each stage might have; all we can assume are a current density  $J$  and certain thermal boundary conditions (heat-sink temperatures or convection boundary conditions), but we can calculate the temperature-dependent thermal conductivity tensor everywhere in the device.

4) Putting it all together (Fig. 3). Based on single-stage simulation, we have created a large table of  $(J, T_L) \rightarrow (Q, F)$  maps. Then, for a given current density level  $J$  and a given set of thermal boundary conditions (heat sink temperatures or convection boundary conditions at exposed facets), we assume a temperature profile throughout the device (e.g., we could assume the whole device to be at the heat-sink temperature). In each stage  $i$ , the  $J$  and the guess for the stage temperature  $T_i$  yield the appropriate heat generation rate in that stage,  $Q_i(J, T_i)$ , based on the table. The temperature-profile guess  $T_i$ , heat generation rate profile  $Q_i$ , and the thermal model yielding the thermal conductivity

tensor everywhere are used in the heat-diffusion equation, which is solved via the standard finite-elements technique to calculate an updated temperature profile. The process is iterated until the obtained temperature profile agrees well with the imposed thermal boundary conditions. After we have established the final temperature profile, we read off the corresponding field profile  $F_i(J, T_i)$  and calculate the total voltage drop across the whole device, which then gives us an  $I$ – $V$  curve directly comparable to experiment.

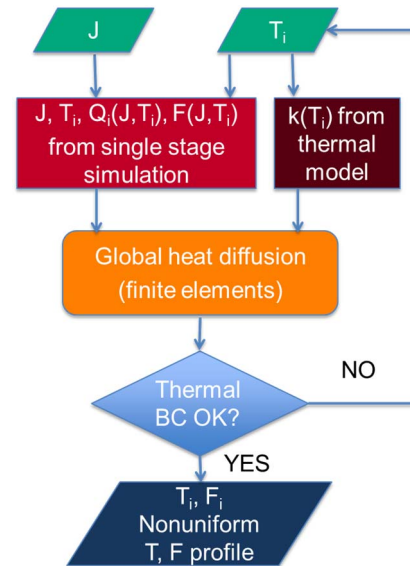


Figure 3: Flowchart of the device-level electrothermal simulation.

In this talk, I will overview our recent work [1-6] on the simulation framework capable of capturing the highly nonequilibrium physics of the strongly coupled electron and phonon systems in quantum cascade lasers and present data for a mid-IR QCL based on this framework.

## REFERENCES

- [1] Y.B. Shi, S. Mei, O. Jonasson, and I. Knezevic, "Modeling quantum cascade lasers: Coupled electron and phonon transport far from equilibrium and across disparate spatial scales," *Fortschr. Phys.* 65, 1600084 (2017).
- [2] S. Mei and I. Knezevic, "Thermal conductivity of III-V semiconductor superlattices," *J. Appl. Phys.* 118, 175101 (2015).
- [3] Y.B. Shi and I. Knezevic, "Nonequilibrium phonon effects in midinfrared quantum cascade lasers," *J. Appl. Phys.* 116, 123105, (2014).
- [4] Y.B. Shi, Z. Aksamija, and I. Knezevic, "Self-Consistent Thermal Simulation of GaAs/Al<sub>0.45</sub>Ga<sub>0.55</sub>As Quantum Cascade Lasers," *J. Comput. Electron.* 11, 144-151 (2012).
- [5] X. Gao, D. Botez, and I. Knezevic, "Monte Carlo modeling of X-valley leakage in quantum cascade lasers," *J. Comput. Electron.* 6, 305-308 (2007).
- [6] X. Gao, D. Botez, and I. Knezevic, "X-valley leakage in GaAs-based mid-infrared quantum cascade lasers: a Monte Carlo study," *J. Appl. Phys.* 101, 063101 (2007).